research articles Journal of proteome research

Identification of Novel 14-3-3ζ Interacting Proteins by Quantitative Immunoprecipitation Combined with Knockdown (QUICK)

Feng Ge,*,† Wen-Liang Li,‡ Li-Jun Bi,§ Sheng-Ce Tao,|| Zhi-Ping Zhang,⊥ and Xian-En Zhang⊥

Institute of Hydrobiology, Chinese Academy of Sciences, Wuhan, Hubei 430072, China, School of Science and Technology, Tokai University, 2-28-4 Tomigaya, Shibuya-ku, Tokyo 1510063, Japan, National Laboratory of Biomacromolecules, Institute of Biophysics, Chinese Academy of Sciences, Beijing 100101, China, Shanghai Center for Systems Biomedicine, Shanghai Jiaotong University, Room126, Wenxuan Building of Medicine, 800 Dongchuan Road, Shanghai 200240, China, and State Key Laboratory of Virology, Wuhan Institute of Virology, Chinese Academy of Sciences, Wuhan 430071, China

Received June 18, 2010

The family of 14-3-3 proteins has emerged as critical regulators of diverse cellular responses under both physiological and pathological conditions. To gain insight into the molecular action of 14-3-3ζ in multiple myeloma (MM), we performed a systematic proteomic analysis of 14-3-3ζ-associated proteins. This analysis, recently developed by Matthias Mann, termed quantitative immunoprecipitation combined with knockdown (QUICK), integrates RNAi, SILAC, immunoprecipitation, and quantitative MS technologies. Quantitative mass spectrometry analysis allowed us to distinguish 14-3-3ζ-interacting proteins from background proteins, resulting in the identification of 292 proteins in total with 95 novel interactions. Three 14-3-3ζ-interacting proteins—BAX, HSP70, and BAG3—were further confirmed by reciprocal coimmunoprecipitations and colocalization analysis. Our results therefore not only uncover a large number of novel 14-3-3ζ-associated proteins that possess a variety of cellular functions, but also provide new research directions for the study of the functions of 14-3-3ζ. This study also demonstrated that QUICK is a useful approach to detect specific protein−protein interactions with very high confidence and may have a wide range of applications in the investigation of protein complex interaction networks.

Keywords: 14-3-3ζ • Quantitative immunoprecipitation combined with knockdown (QUICK) • Multiple myeloma (MM) • BCL2-associated athanogene 3 (BAG3) • BCL2-associated X protein (BAX)

Introduction

The 14-3-3 proteins have emerged as critical regulators of diverse cellular responses in eukaryotic organisms.[1−3] In mammalian cells, seven different isoforms (ζ, β, γ, ε, σ, η and θ) have been identified with distinct tissue localization and function for each isoform. The 14-3-3 proteins self-assemble into homo- and heterodimers, with some family members, such as σ and γ, preferring to homodimerize and other family members, such as ε, preferring to heterodimerize.[4] The 14-3-3 dimers are able to function as an adapter, linker, scaffold, or coordinator in assembling signaling complexes.[5−7] Through interacting with more than 400 target proteins identified so far, these 14-3-3 proteins are known to be involved in widespread biological processes such as signal transduction, cell cycle control, apoptosis, cellular metabolism, proliferation, cytoskeletal regulation, transcription, and redox-regulation or stress response.[8,9] For example, 14-3-3 proteins associate with a number of different signaling proteins including MEKK1, and PI-3 kinase,[10,11] apoptosis regulatory proteins ASK-1 and tumor suppressor p53,[12−14] transcription regulatory protein FKHRL1 and DAF-16 and histone deacetylase.[15−17] The 14-3-3 proteins promote cell survival through their interactions with signaling proteins such as EGFR, Raf-1, the pro-apoptotic protein BAD, and the cell cycle phosphatase cdc25.[18,19] Furthermore, 14-3-3s may have multiple roles in connecting signaling pathways to the regulation of actin-based cellular changes in cytoskeleton and cell motility.[20] The 14-3-3 proteins associate with so many different molecules in large part because of their specific phosphoserine/phosphothreonine-binding activity.[21] Detailed analysis of interactions between 14-3-3 proteins and their targets and the use of an oriented peptide library screening approaches resulted in identification of three optimal 14-3-3 binding motifs: RSXpSXP (mode 1), RXXXpSXP (mode 2),[1,22] and (pS/pT)X_{1-2}-COOH (mode 3),[23] where pS represents phospho-serine and X denotes any amino acid residues except cysteine. However, it is important to note that not all phos-

* Corresponding author: Prof. Feng Ge, Institute of Hydrobiology, Chinese Academy of Sciences, Wuhan, Hubei 430072, China. Tel/Fax: +86-27-68780500. E-mail: gefeng@ihb.ac.cn.
† Institute of Hydrobiology, Chinese Academy of Sciences.
‡ Tokai University.
§ National Laboratory of Biomacromolecules, Institute of Biophysics, Chinese Academy of Sciences.
|| Shanghai Jiaotong University.
⊥ State Key Laboratory of Virology, Wuhan Institute of Virology, Chinese Academy of Sciences.

Published on Web 09/29/2010
10.1021/pr100616g

phorylation-dependent sites conform to these motifs[24] and not all interactions are phosphorylation-dependent.[25,26]

In general, 14-3-3 proteins play a role in promoting survival and repressing apoptosis.[12] However, each isoform may have unique functions in certain physiological contexts. For example, 14-3-3ζ, also termed as YWHAZ (tyrosine 3-monooxygenase/tryptophan 5-monooxygenase activation protein, zeta polypeptide), has been shown to facilitate transactivation of β-catenin by the survival kinase AKT,[27] and colocalize with activated Akt in intestinal stem cells (ISCs), suggesting the involvement of 14-3-3ζ in stem cell development and tumorigenesis. Li et al. reported that knockdown of 14-3-3ζ in lung cancer cells led to inhibition of the anchorage-independent growth of these cells and to cause increased apoptosis when cells were detached from the plate matrix, a phenomenon known as anoikis.[28] Work by Lu and colleagues observed that 14-3-3ζ overexpression can reduce cell adhesion and induce epithelial−mesenchymal transition.[29] Thus, the conclusion from these studies is that upregulation of 14-3-3ζ can help tumor cells resist apoptosis and might provide them with an increased potential for tumor invasion and metastasis.

In our previous study, comparative proteomics was performed to look at As_2O_3-induced apoptosis in multiple myeloma (MM) cells. By comparing the protein profiles of MM cells treated by As_2O_3 with those of untreated control, 14-3-3ζ was identified as a potential therapeutic target.[30] However, the molecular mechanism of 14-3-3ζ in MM pathogenesis is still unclear. A systemic identification of novel 14-3-3ζ protein interactions may provide new clues about the molecular mechanism of 14-3-3ζ in MM pathogenesis.

To address the technical concerns about the sensitivity and accuracy of profiling protein−protein interactions (PPIs) for 14-3-3ζ, we applied the technology developed by Matthias Mann,[31] namely, using a method that combines stable isotope labeling with amino acids (SILAC),[32,33] RNAi-induced knockdown, coimmunoprecipitation, and quantitative MS. This method was termed as quantitative immunoprecipitation combined with knockdown (QUICK).[31] With QUICK, cells are metabolically labeled by SILAC method, the protein of interest is knocked down by RNAi in one of two samples, and cell lysates of untreated and knockdown cells are incubated with an immobilized antibody against the protein of interest and the precipitated proteins are analyzed by mass spectrometry. The target protein itself and its interaction partners should be more abundant in the untreated cells than those in the knockdown cells, while contaminating proteins should be present in similar amounts in both untreated and knockdown cells. This highly sensitive and accurate approach for PPI analysis has been applied to identify interaction partners of β-catenin and Cbl in colon carcinoma cells[31] and the novel interaction partners of vesicle-inducing protein in plastids 1 (VIPP1) in *Chlamydomonas*.[34]

In this study, QUICK method was undertaken to identify proteins that bind to 14-3-3ζ at endogenous level. Measures were taken to improve the assay. First, *in vivo* cross-linking using formaldehyde was carried out to fix protein interactions prior to cell lysis, which can stabilize weak and transient interactions during purification processes. Second, we modified the sample mixture strategy before purification. That is, equal amount of two groups of cellular proteins respectively extracted from heavy [$^{13}C_6$] or light [$^{12}C_6$] L-lysine labeled cells was mixed before purification, and the mixture was affinity-purified with anti-14-3-3ζ antibody. Our "purification after mix" method allowed purification to be performed under identical conditions to minimize the deviation of SILAC quantitation. Third, to eliminate the nonspecific purification background (i.e., proteins bound to affinity resins nonspecifically) and prevent the formation of noncovalent interactions after cell lysis, an internal control allowing for the correction of unequal immunoprecipitation and/or labeling efficiencies was included. By using this modified QUICK strategy, a total of 292 proteins were identified and 95 of them were novel 14-3-3ζ putative partners. Our results revealed the functional diversity of 14-3-3ζ and provided a number of new research directions in the study of 14-3-3ζ biology. This study also demonstrated that QUICK is a useful method to detect specific protein−protein interactions with very high confidence and offers substantial advantages over other approaches.

Experimental Procedures

Cell Culture, RNAi and SILAC. The human myeloma cell line U266 was purchased from American Type Culture Collections (Rockville, MD). Myeloma cells were routinely maintained in RPMI 1640 supplemented with 1% penicillin/streptomycin, 1 mmol/L L-glutamine, and 10% fetal bovine serum at 37 °C, 5% CO_2 in air.

14-3-3ζ gene silencing was performed by transfecting U266 cells with a plasmid in which the cloned DNA fragment acts as template for the synthesis of small interfering RNA molecules by using pGPU6/Neo siRNA Expression Vector kit (GenePharma Co., Shanghai, China). The siRNA targeting 14-3-3ζ sequence was used as described previously.[30] Moreover, a negative control scrambled siRNA (5′-TTCTCCGAACGTGTCACGTTT-3′), which has no significant homology to human gene sequences, was taken as a control. The resulting pGPU6/Neo/YWHAZ and pGPU6/Neo/control vectors were purified and used to transfect the U266 cells as described previously.[30] Transfected cells were selected for neomycin resistance for 2 weeks. One clone was selected from pGPU6/Neo/control transfected U266 cells (designated as U266-NC) and one from pGPU6/Neo/YWHAZ transfected U266 cells (designated as U266-KD). Changes in 14-3-3ζ protein levels were determined by Western blot analysis as described.[30]

For SILAC experiments, the SILAC Protein Quantitation Kit (Pierce Biotechnology, Rockford, IL) was used according to the manufacturer's instruction. In brief, U266-KD or U266-NC cells were grown in SILAC RPMI 1640 Medium (Pierce) containing 10% (v/v) dialyzed FBS, and 0.1 mg/mL heavy [$^{13}C_6$] or light [$^{12}C_6$] L-lysine, respectively. To ensure full incorporation of the heavy and light labeled amino acids, cells were grown for at least six cell doublings prior to treatment. In parallel, a control experiment was performed by culturing U266-NC cells in 'Heavy' ([$^{13}C_6$] L-lysine) media.

***In Vivo* Formaldehyde Cross-Linking.** U266-NC or U266-KD cells were harvested, washed with PBS, and incubated in 1.0% (w/v) paraformaldehyde (PFA) in PBS for 10 min at 37 °C. To stop the cross-linking reaction, 1.25 M glycine was added to a final concentration of 125 mM for 5 min at room temperature (RT). Cells were harvested, washed three times with ice-cold washing buffer (10 üM Tris-HCl, 250 μM sucrose, pH 7.0), and transferred to a clean 1.5 mL Eppendorf tube. Cells were lysed with RIPA lysis buffer (50 mM Tris-HCl, 150 mM NaCl, 0.1% SDS, 1% NP-40, 0.5% sodium deoxycholate, 1 mM PMSF, 100 mM leupeptin, and 2 mg/mL aprotinin, pH 8.0). Cellular debris was removed by centrifugation for 30 min at 13 200*g* and at 4 °C. Supernatants were collected and protein

concentrations were measured in duplicate using a BCA protein assay kit (Pierce).

Antibody Coupling and Immunoprecipitation. To prevent interference of excess of antibodies with mass spectrometric detection, the 14-3-3ζ antibody was coupled to Protein A Sepharose CL-4B (GE Healthcare Biosciences, Sweden). Protein A Sepharose CL-4B was mixed with antibody in 0.1 M borate buffer, pH 8.2, for 30 min at RT with gentle shaking, after which the Sepharose beads were washed with excess borate buffer. The Sepharose was washed with 0.2 M triethanolamine, pH 8.2, and then resuspended in 20 vol of dimethyl pimelimidate dihydrochloride (Pierce) freshly made up in 0.2 M triethanolamine with the pH readjusted to pH 8.2. The mixture was agitated gently at RT for 1 h and the reaction was stopped by centrifuging the beads (500*g* for 1 min) and resuspending in an equal volume of ethanolamine, pH 8.2, of the same molarity as the dimethyl pimelimidate dihydrochloride. After 5 min, the cross-linked beads were centrifuged and washed three times with lysis buffer.

Prior to immunoprecipitation, 2 mg of protein from light [$^{12}C_6$] L-lysine labeled U266-NC cells was mixed with 2 mg of protein from heavy [$^{13}C_6$] L-lysine labeled U266-KD (siRNA group) or U266-NC cells (control group), respectively, and precleared with 0.2 mL of Protein A Sepharose for 2 h. Protein A-sepharose beads with coupled antibodies were split and mixed with precleared mixtures and rotated for 18 h at 4 °C. The beads were washed twice with 2 mL of lysis buffer containing 0.1% Triton X-100, and two times with 2 mL of lysis buffer without detergent. After complete removal of the supernatant with a microliter syringe, immunoprecipitated proteins were eluted with 3 × 200 μL of 5% acetic acid, pH 3, and speed-vacuum-dried. Laemelli sample buffer, pH = 7.4 (10 mM Tris, 10% (v/v) glycerol, 2% (w/v) SDS, 5 mM EDTA, 0.02% bromophenol blue and 6% β-mercaptoethanol) was added and boiled for 20 min at 95 °C. Proteins were then separated on a 10% SDS-PAGE gel and visualized with Coomassie blue staining.

Protein Separation and In-Gel Digestion. Protein bands were excised from the SDS-PAGE gel and cut into 40 sections for in-gel tryptic digestion. The excised sections were chopped into small particles and washed in water and completely destained using 100 mM ammonium bicarbonate in 50% acetonitrile (ACN). A reduction step was performed by addition of 100 μL of 10 mM dithiothreitol (DTT) at 37 °C for 1 h. The proteins were alkylated by adding 100 μL of 50 mM iodoacetamide and allowed to react in the dark at RT for 1 h. Gel sections were first washed in water, then acetonitrile, and finally dried by SpeedVac (Thermo Fisher Scientific, Waltham, MA) for 30 min. Digestion was carried out using 20 μg/mL sequencing grade modified trypsin (Promega) in 50 mM ammonium bicarbonate. Sufficient trypsin solution was added to swell the gel pieces, which were kept at 4 °C for 45 min and then incubated at 37 °C overnight. The supernatants were transferred into a 200 μL microcentrifuge tube and the gels were extracted once with extraction buffer (67% acetonitrile containing 2.5% trifluoroacetic acid). The peptide extract and the supernatant of the gel slice were combined and then finally concentrated to a volume of as little as 20 μL to inject into the nanoLC system.

Mass Spectrometry, Protein Identification, and Quantification. After application of the peptide mixture to a C-18 column (800 μm i.d. × 3 mm long), reversed-phase separation of the captured peptides was done on a column (150 μm i.d. × 75 mm long) filled with HiQ sil C-18 (3-μm particles, 120-Å pores, KYA technologies) using a direct nanoflow LC system (Dina, KYA Technologies). The peptides were eluted with a linear 5−65% gradient of acetonitrile containing 0.1% formic acid over 120 min at a flow rate of 200 nL/min and sprayed into a quadrupole time-of-flight tandem mass spectrometer (Q-TOF-2, Micromass). Acquisition of MS/MS spectra was performed using the parameters as indicated below: dynamic exclusion time, 120 s; duty cycle, 2 s; mass tolerance, 0.1 Da. The MS/MS signals were then converted to text files by MassLynx (version 3.5, Micromass) and processed against the IPI.HUMAN 3.49 database (74 017 protein entries) using the Mascot algorithm (version 2.2.04, Matrix Science) with the following parameters: fixed modification, carbamidomethylation (Cys); variable modifications, oxidation (Met), stable isotopes of Lys; maximum missed cleavages, 2; peptide mass tolerance, 500 ppm; MS/MS tolerance, 0.5 Da. Protein identification was based on the criterion of having at least one MS/MS data with Mascot scores that exceeded the thresholds ($p < 0.05$). A randomized decoy database created by a Mascot Perl program estimated a false discovery rate at 0.96% for all the identified peptides and 0.78% on the protein level. Relative abundance of each peptide was determined by using the AYUMS algorithm (version 1.00).[35] Only proteins with a minimum of 2 quantifiable peptides were included in our final data set.

As potential interaction partners of 14-3-3ζ are expected to have a higher SILAC ration in the siRNA group than in control group, we excluded proteins that had similar SILAC ratios in both experiments. We conservatively set the cutoff SI ratio (SI = SILAC ratio of siRNA group/SILAC ratio of control group) at 2 as the threshold for determining 14-3-3ζ-interacting proteins (e.g., a protein was defined as a 14-3-3ζ-interacting protein if its SI value ≥2).

Protein Categorization. All identified proteins were classified based on the PANTHER (Protein ANalysis THrough Evolutionary Relationships) system (http://www.pantherdb.org), which is a unique resource that classifies genes and proteins by their functions.[36]

Western Blot Analysis. Protein extracts (30 μg) prepared with RIPA lysis buffer (50 mM Tris-HCl, 150 mM NaCl, 0.1% SDS, 1% NP-40, 0.5% sodium deoxycholate, 1 mM PMSF, 100 mM leupeptin, and 2 mg/mL aprotinin, pH 8.0) were resolved by a 10% SDS-PAGE gel, and transferred onto an Immobilon-P PVDF transfer membrane (Millipore, Bedford, MA) by electroblotting. After blocking with 5% nonfat milk, the membranes were probed with rabbit anti-14-3-3γ polyclonal, rabbit anti-14-3-3η polyclonal antibodies (Cell Signaling, Danvers, MA), rabbit anti-pan 14-3-3 polyclonal, rabbit anti-14-3-3ζ polyclonal, rabbit anti-14-3-3ε polyclonal, goat anti-14-3-3σ polyclonal, mouse anti-14-3-3θ monoclonal, mouse anti-14-3-3β monoclonal, and mouse anti-GAPDH monoclonal antibodies (Santa Cruz Biotechnology, Santa Cruz, CA). Blots were then incubated with a streptavidin alkaline phosphatase-conjugate secondary antibody (Amersham Biosciences, Piscataway, NJ) for 1 h at RT. The signal was visualized with ECL detection reagent (GE Healthcare Biosciences, Sweden).

Coimmunoprecipitation and Western Blot Analysis. Cell lysates were prepared as described above. Thereafter, lysates were precleared by Protein A/G Plus beads (Santa Cruz Biotechnology) followed by incubation with rabbit anti-14-3-3ζ polyclonal, rabbit anti-BAX polyclonal antibodies (Santa Cruz Biotechnology), rabbit anti-HSP70 polyclonal antibody (Cell Signaling), or rabbit anti-BAG3 polyclonal antibody (Abcam, Inc., Cambridge, MA) (at a dilution of 1:100) overnight

on a rocker at 4 °C. Immune complexes were pulled down by incubating with Protein A/G Plus beads for 4 h at 4 °C followed by washing twice with lysis buffer containing 0.1% Triton X-100, and two times with lysis buffer without detergent. Protein A/G Plus beads bound immune-complexes were then resuspended in 1× Laemelli sample buffer, boiled for 5 min, and analyzed by Western blotting using specific antibodies as described above.

Confocal Fluorescence Microscopy. The U266 cells grown on poly L-lysine-treated glass coverslips were transfected with pEGFP-14-3-3ζ plasmid as previously described.[30] Twenty-four hours after transfection, cells were fixed with 4% paraformaldehyde and permeabilized by 0.1% Triton X-100. After a brief washing in PBS, slides were blocked with 1% BSA for 1 h and then incubated with the anti-BAX, HSP70, or BAG3 antibody at a dilution of 1:400. The cells were then washed three times with PBS and incubated with Alexa fluor594-conjugated secondary antibody (Invitrogen, Carlsbad, CA) at a dilution of 1:400 for 1 h. After that, cells were washed and mounted, and examined using LSM 710 laser scanning confocal microscope (Carl Zeiss, Jena, Germany). Images were taken with the 63× oil immersion objective lenses at identical imaging settings.

Colocalization Image Analysis. The colocalization analysis was performed on paired images using the NIH Image J software (National Institutes of Health, Bethesda, MD) and JACoP plug-in.[37] Pearson's correlation and overlap coefficients according to Mander's were calculated from those images. The Mander's coefficients range from 0 to 1 and are independent of the pixel intensities within the individual channels.[37] Pearson's correlation coefficient (*R*) was determined by JACoP plug-in and the Colocalization Test tool was used to generate random images using an approach described by Costes et al.[38] The scrambled images from the second channel are compared with the first channel to determine if the colocalization occurs as a matter of chance. To generate the scrambled images, blocks of pixels are rearranged at random and the Pearson's *R* is calculated for each new random image. For each comparison, 3000 such random images were generated, and the values of the random *R* (*R*(rand)) were compared with the actual *R*.[38]

Results

Identification of 14-3-3ζ Interacting Proteins. The QUICK method is a SILAC-based quantitative strategy to capture endogenous PPIs with very high confidence.[31] The strategy for purification and identification of interacting proteins associated with 14-3-3ζ using the QUICK method was mainly illustrated in Figure 1. A prerequisite for the QUICK assay is the availability of RNAi cells exhibiting reduced expression of the protein for which interaction partners are to be identified. As shown in Figure 2, 14-3-3ζ knockdown U266 cells (U266-KD) showed diminished 14-3-3ζ protein levels comparing with the parental U266 and U266 transfected with negative control siRNA (U266-NC). Depletion of intracellular 14-3-3ζ showed no obvious effect on the expression of other 14-3-3 isoforms and internal control GAPDH (Figure 2).

In this study, U266-KD or U266-NC cells are metabolically labeled via the SILAC method by growing them in medium containing either light or heavy stable isotopes of lysine. Since formaldehyde is a reversible cross-linker that efficiently produces protein−protein cross-links *in vivo* and protein complexes in cell extracts were specifically stabilized by this cross-linker,[39,40] formaldehyde was added prior to cell lysis. Equal amounts of cell lysates from cells that are differentially

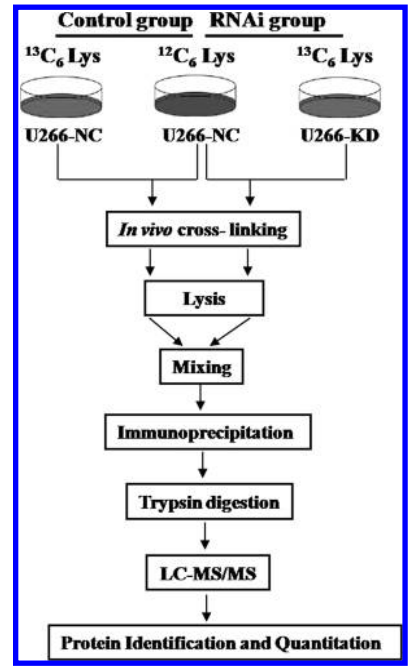

Figure 1. Schematic diagram of a quantitative strategy using SILAC coupled with *in vivo* cross-linking and RNAi to identify specific 14-3-3ζ-interacting proteins. U266-NC and U266-KD cells were differentially labeled by growing them in medium containing light or heavy amino acids (SILAC). Cells were lysed, combined, immunoprecipitated, and analyzed by quantitative proteomics (LC−MS/MS). The 14-3-3ζ interaction partners were detected by their higher abundance in the light form. In parallel, a control experiment was performed by culturing two populations of U266-NC cells in light and heavy media, respectively, which should have a SILAC ratio of 1:1 for all identified proteins.

labeled are mixed and incubated with an immobilized antibody against 14-3-3ζ. The precipitated proteins are eluted, digested, and then identified by LC−MS, and the proteins specifically interacting with 14-3-3ζ were distinguished from nonspecific protein background according to the quantitative criteria as described in Experimental Procedures.

As expected, 14-3-3ζ was identified as one of the components of the precipitates with sequence coverage of more than 50% (Table S4 in Supporting Information). According to the criteria described in Experimental Procedures, a total of 292 proteins were identified to interact with 14-3-3ζ after removing proteins that were not found in the control group, and subtracting proteins with SI ratio <2 (Table S1). Among all quantified proteins, 51 were identified as background proteins (Table S2). The lists of all quantified proteins in RNAi or control group are shown in Tables S3 and S4, respectively. Comparison of our data set with 456 known interacting proteins of 14-3-3ζ (http://www.genecards.org/cgi-bin/carddisp.pl?gene=YWHAZ&search=YWHAZ&rf=/home/genecards/current/website/carddisp.pl&interactions=456#int) (Table S5) revealed significant overlap but also differences (Tables S1 and S2). About 67% of the proteins identified in this study have been reported in previous large-scale studies and 95 proteins were newly identified 14-3-3ζ interacting partners (Table 1). It is worth mentioning that six previously reported putative 14-3-3ζ binding partners, GAPDH, regulator of nonsense transcripts 1 (UPF1), fructose-bisphosphate aldolase A (ALDOA), L-lactate dehydrogenase A chain (LDHA), L-lactate dehydrogenase B chain

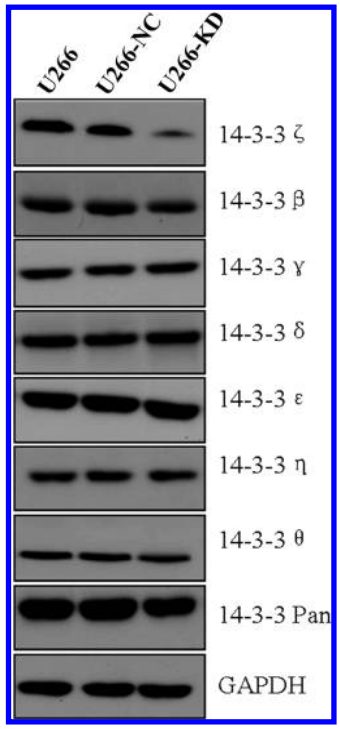

Figure 2. Expression of 14-3-3 isoforms in U266 parental (U266) and control cells (NC) and U266/14-3-3ζ shRNA cells (KD). Compared with the parental U266 and U266-NC cells, U266-KD cells showed diminished 14-3-3ζ protein levels. Depletion of 14-3-3ζ showed no obvious effect on the expression of other 14-3-3 isoforms. GAPDH blotting was performed to ensure equal loading.

(LDHB), and uncharacterized protein MVP, had SI value close to 1, indicating that under our experimental conditions they are likely nonspecific interacting proteins. The novel proteins identified in our experiment might be a result of differences in cell lines, cell culture conditions, purification strategies, and mass spectrometry platforms used.

Categorization of the Novel 14-3-3ζ Interacting Proteins. To understand the biological relevance of the novel 14-3-3ζ interacting proteins, PANTHER classification system was used to classify these novel interactors according to their functions. The PANTHER classification system revealed that the interactors can be classified into 11 groups according to their functions (Figure 3). The largest group of novel 14-3-3ζ-interacting proteins is involved in protein metabolism (33%). Significant numbers of 14-3-3ζ targets are also implicated in apoptosis (10%), signal transduction (11%), and nucleic acid binding (7%), indicating that 14-3-3ζ is the critical regulator of diverse cellular functions involving widespread biological processes.

Validation of the 14-3-3ζ Interacting Proteins by Reciprocal Immunoprecipitation. To validate some of the proteins identified by MS, coimmunoprecipitation experiments and Western blot analysis were performed. On the basis of how well their biological functions and importance are known, we selected two novel, putative 14-3-3ζ binding proteins for validation. We also included one protein, HSP70, which has been previously reported to physically interact with 14-3-3ζ as a positive control for these coimmunoprecipitation experiments. As shown in Figure 4 A, 14-3-3ζ, BAX, HSP70, and BAG3 were detected in the 14-3-3ζ immune complex (14-3-3ζ) and the U266 cell lysate (Input) but not in the nonimmune IgG control (IgG). Furthermore, reverse immunoprecipitation assay using specific antibodies for these proteins followed by Western blotting with BAX (Figure 4B), HSP70 (Figure 4C), and BAG3 (Figure 4D) confirmed their binding to 14-3-3ζ. Thus, compelling evidence shows that 14-3-3ζ interacts with BAX, HSP70, and BAG3 proteins in MM cells.

Confocal Immunofluorescence Analysis. As an independent approach, we used confocal immunofluorescence microscopy to investigate the colocalization of 14-3-3ζ with BAX, HSP70, and BAG3 in U266 cells. Immunofluorescence assays revealed that BAX, HSP70, and BAG3 had a tendency to appear coclustered with 14-3-3ζ in the U266 cells (Figure 5). Importantly, Table 2 summarizes statistical colocalization metrics of respective analyses of pairwise protein comparisons. The statistical analyses in Table 2 of the images in Figure 5 demonstrate rigorously the colocalization of 14-3-3ζ with BAX, HSP70, and BAG3 in U266 cells. Altogether, these results demonstrated that 14-3-3ζ can interact with BAX, HSP70, and BAG3 in MM cells.

Discussion

In our previous study, we found that RNAi-based 14-3-3ζ knockdown can lead to induction of apoptosis in MM cells.[30] However, the functions of 14-3-3ζ in MM cells remain poorly understood and the mechanistic aspects of how 14-3-3ζ accomplishes its functions remain somewhat enigmatic and controversial. To address this point, we have performed a comprehensive analysis of the interactome of 14-3-3ζ in myeloma cells using the QUICK method. As a result, a total of 292 14-3-3ζ interacting proteins were unambiguously identified with very high confidence. Importantly, the current study also revealed a number of novel 14-3-3ζ binding partners. Furthermore, the interaction of 14-3-3ζ with BAX, HSP70, and BAG3 was confirmed by coimmunoprecipitation combined with Western blot analysis and colocalization analysis. The PANTHER classification system revealed that these novel 14-3-3ζ interacting proteins were involved in protein metabolism, signal transduction, apoptosis, and so on, suggesting the functional diversity of 14-3-3ζ (Figure 3).

The protein metabolism class contains 31 novel interacting proteins, including BCL2-associated athanogene 3 (BAG3). The human BAG protein family comprises six family members (BAG1−6) that are thought to function as molecular chaperone regulators.[41] BAG proteins have been shown to participate in a wide variety of cellular processes including cell survival (stress response), proliferation, migration, and apoptosis.[41] BAG3, also known as CAIR-1 or Bis,[42] is involved in a number of activities including the regulation of apoptosis in cancer cells,[43] as well as in proteasomal degradation of ubiquitinated proteins,[44] in the regulation of macroautophagic protein degradation in aging cells,[45] and virus replication.[46]

BAG family proteins have been suggested to function primarily via a conserved BAG domain that interacts with heat-shock proteins (HSP70).[41,47] HSP70 is a chaperone protein expressed constitutively under normal conditions to maintain protein homeostasis and are induced upon environmental stress.[48] A wide variety of signal-transducing proteins of relevance to cancer have been reported to be regulated either directly by HSP70 or indirectly through HSP90-HSP70 interactions, including the protein tyrosine kinase Src, the serine/threonine kinase Raf-1, and the tumor suppressors p53 and WT-1.[49]

Previous studies indicated that 14-3-3ζ can bind to heat shock proteins and HSP70 is one of its binding partners.[50] Consistent with this report, 11 heat shock proteins were

Table 1. List of Novel 14-3-3ζ Interacting Proteins Identified by QUICK Method

		control group		siRNA group		
gene name	description	SILAC ratio (Sc)	SD	SILAC ratio (Si)	SD	SI = Si/Sc
	Signal Transduction					
CLIC1	Chloride intracellular channel protein 1	1.13	0.04	3.67	0.02	3.25
CSNK2A1	Casein kinase II subunit alpha	1.08	0.06	2.19	0.13	2.03
STAT3	Signal transducer and activator of transcription 3 isoform 3	1.08	0.04	2.25	0.09	2.08
MX1	Interferon-induced GTP-binding protein Mx1	0.98	0.06	3.08	0.06	3.14
STAT5A	Signal transducer and activator of transcription 5A	1.03	0.09	2.55	0.06	2.48
STAT5B	Signal transducer and activator of transcription 5B	0.99	0.04	3.02	0.1	3.05
PPM1G	Protein phosphatase 1G	0.95	0.07	2.48	0.1	2.61
PABPC1	Polyadenylate-binding protein 1	1.24	0.04	4.89	0.17	3.94
GDI2	Rab GDP dissociation inhibitor beta	1.09	0.03	2.52	0.07	2.31
ITGB1	Integrin beta 1	0.92	0.02	3.76	0.26	4.09
GNAI2	Guanine nucleotide-binding protein G, alpha-2 subunit	0.98	0.07	12.02	0.41	12.27
	Apoptosis					
HDAC1	Histone deacetylase 1	1.03	0	4.36	0.12	4.23
HDAC2	Histone deacetylase 2	1.26	0.02	4.62	0.07	3.67
ARHGEF2	Rho/rac guanine nucleotide exchange factor 2	0.95	0.01	2.62	0.19	2.76
CASP3	Caspase-3	0.98	0.08	2.97	0.1	3.03
CASP4	Caspase-4	0.98	0.02	2.58	0.02	2.63
CASP6	Caspase-6	1.03	0.07	4.18	0	4.06
COP1	Caspase-1 inhibitor COP	1.03	0.07	5.78	0	5.61
CYCS	Cytochrome c	1.14	0.18	3.59	0.09	3.15
PPP1CA	Serine/threonine-protein phosphatase PP1-alpha catalytic subunit	1.12	0.01	3.63	1.05	3.24
BAX	BCL2-associated X protein	1	0.05	2.44	0.09	2.44
	Protein Metabolism					
BAG2	BAG family molecular chaperone regulator 2	1.06	0.03	3.35	0.02	3.16
BAG3	BAG family molecular chaperone regulator 3	0.99	0.06	3.93	0	3.97
USP14	Ubiquitin carboxyl-terminal hydrolase 14	1.11	0.18	3.44	0.11	3.1
USP15	Ubiquitin carboxyl-terminal hydrolase 15	0.96	0.03	2.01	0.34	2.09
USP47	Ubiquitin carboxyl-terminal hydrolase 47	0.95	0.01	2.38	0.5	2.51
USP5	Ubiquitin carboxyl-terminal hydrolase 5	1.26	0.07	2.75	0.16	2.18
STIP1	Stress-induced-phosphoprotein 1	1.14	0.09	3.47	0.06	3.04
PSMB1	Proteasome subunit beta type-1	1.14	0.05	3.76	0.06	3.3
PSMB2	Proteasome subunit beta type-2	0.91	0.04	2.86	0.04	3.14
PSMB4	Proteasome subunit beta type-4	1.22	0.12	4.8	0.02	3.93
PSMB5	Proteasome subunit beta type-5	1.06	0.14	3.8	0	3.58
PSMB8	Proteasome subunit beta type-8	0.97	0	3.99	0	4.11
PSMD10	Proteasome 26S non- ATPase subunit 10	1.04	0.05	3.08	0	2.96
PSMD11	Proteasome 26S non-ATPase subunit 11	1.05	0.08	3.4	0.08	3.24
PSMD12	26S proteasome non-ATPase regulatory subunit 12	1.06	0.05	4.19	0.13	3.95
PSMD13	26S proteasome regulatory subunit S11	1.18	0.05	3.19	0.08	2.7
PSMD14	26S proteasome non-ATPase regulatory subunit 14	1	0.12	3.46	0.06	3.46
PSMD3	26S proteasome non-ATPase regulatory subunit 3	1.23	0.07	3.57	0.22	2.9
PSMD5	26S proteasome non-ATPase regulatory subunit 5	1.01	0.14	2.65	0.05	2.62
PSMD7	26S proteasome non-ATPase regulatory subunit 7	0.93	0	3.35	0.09	3.6
PSMD8	Proteasome 26S non-ATPase subunit 8	1.16	0.06	3.43	0.15	2.96
CCT5	T-complex protein 1 subunit epsilon	1.05	0.01	3.6	0.08	3.43
UBA2	SUMO-activating enzyme subunit 2	1.09	0.12	3.05	0.21	2.8
RPL13A	60S ribosomal protein L13a	1.08	0.19	5.69	0.24	5.27
RPL36	60S ribosomal protein L36	0.96	0.09	3.22	0.04	3.35
EIF3B	Eukaryotic translation initiation factor 3 subunit B	1.03	0.01	3.46	0.17	3.36
EIF3D	Eukaryotic translation initiation factor 3 subunit D	1.07	0.04	3.54	0.06	3.31
EIF3E	Eukaryotic translation initiation factor 3 subunit E	1.28	0.04	5.43	0.12	4.24
EIF3K	Eukaryotic translation initiation factor 3 subunit K	1.29	0.11	3.43	0.11	2.66
EIF3M	Eukaryotic translation initiation factor 3 subunit M	1.28	0.03	3.33	0.07	2.6
GPS1	G protein pathway suppressor 1	1.11	0.08	3.41	0.24	3.07

Table 1. Continued

gene name	description	control group SILAC ratio (Sc)	SD	siRNA group SILAC ratio (Si)	SD	SI = Si/Sc
	Cytoskeleton					
EPB41L2	Band 4.1-like protein 2	1.1	0.03	2.55	0.25	2.32
MYH10	Myosin-10	1.11	0.1	3.4	0.12	3.06
MYH9	Myosin-9	0.97	0.05	2.02	0.19	2.08
MAPRE1	Microtubule-associated protein RP/EB family member 1	1.1	0.06	3.16	0.04	2.87
	Cell Cycle					
RAB5C	Ras-related protein Rab-5C	1.18	0.37	5.35	0.02	4.53
RAB1A	Ras-related protein Rab-1A	1.18	0.04	3.47	0.11	2.94
RAB14	Ras-related protein Rab-14	1.19	0.06	4.38	0.3	3.68
MCM2	DNA replication licensing factor MCM2	1.2	0.15	2.44	0.13	2.03
MCM4	DNA replication licensing factor MCM4	1.23	0.01	3.59	0.35	2.92
MCM7	DNA replication licensing factor MCM7	1.17	0.1	3.26	0.02	2.79
DUSP3	Dual specificity protein phosphatase 3	0.97	0.04	4.28	0.03	4.41
	Protein Transport					
FLOT1	Flotillin-1	1	0	4.45	0.32	4.45
CLTCL1	Clathrin heavy chain 2	0.96	0.05	2.65	0.21	2.76
ANXA5	Annexin A5	1.15	0.04	3.22	0.02	2.8
ANXA6	Annexin A6	1.15	0.3	3.42	0.11	2.97
ANXA11	Annexin A11	1.07	0	4.41	0.2	4.12
	Nucleic Acid Binding					
PARP1	Poly [ADP-ribose] polymerase 1	1.03	0.09	19.78	4.07	19.2
MATR3	Matrin-3	0.93	0.06	3.84	0.43	4.13
RSU1	Ras suppressor protein 1	1.19	0.06	2.54	0.09	2.13
ADSS	Adenylosuccinate synthetase isozyme 2	0.97	0.05	3.4	0.21	3.51
TP53BP1	Tumor suppressor p53-binding protein 1	1.01	0.07	2.69	0.08	2.66
MSH6	DNA mismatch repair protein Msh6	1.05	0.02	3.62	0.39	3.45
DCPS	Scavenger mRNA-decapping enzyme DcpS	1.04	0	4.83	0.14	4.64
	Cell Adhesion					
LAMC1	Laminin subunit gamma-1	1.07	0.09	2.95	0.05	2.76
RAB1B	Ras-related protein Rab-1B	1.2	0.03	3.21	0.11	2.68
RAB7A	Ras-related protein Rab-7a	1.04	0.02	3.22	0.07	3.1
RAP1A	Ras-related protein Rap-1A	1.05	0.11	3.56	0.31	3.39
RAP1B	Ras-related protein Rap-1b	1.05	0.22	3.64	0.29	3.47
PTPN1	Tyrosine-protein phosphatase nonreceptor type 1	1.12	0.03	4.28	0.03	3.82
	Peroxidase					
PRDX2	Peroxiredoxin-2	0.96	0.08	2.67	0.08	2.78
PRDX3	Thioredoxin-dependent peroxide reductase, mitochondrial	1.01	0.3	3.37	0.05	3.34
PRDX4	Peroxiredoxin-4	1.26	0.08	3.5	0.05	2.78
PRDX5	Peroxiredoxin-5	1.21	0.08	3.86	0.26	3.19
PRDX6	Peroxiredoxin-6	1.11	0.05	3.52	0.06	3.17
	Function Unclassified					
ATXN10	Ataxin-10	0.94	0.04	4.33	0	4.61
SMCHD1	Structural maintenance of chromosomes flexible hinge domain-containing protein 1	1.04	0.08	3.62	0.39	3.48
TPD52L2	Tumor protein D52-like 2	0.96	0.09	3.16	0.11	3.29
	Kinase					
MAP3K4	Mitogen-activated protein kinase kinase kinase 4 isoform a	1.04	0.02	2.82	0	2.71
MAPK1	Mitogen-activated protein kinase 1	0.97	0.06	4.28	0	4.41
MAPK3	Mitogen-activated protein kinase 3	1.04	0.04	4.28	0	4.12
MAPKSP1	Mitogen-activated protein kinase kinase 1-interacting protein 1	1.09	0.08	3.89	0	3.57
PDXK	Pyridoxal kinase	1.06	0.02	2.37	0.15	2.24
PAK2	Serine/threonine-protein kinase PAK 2	1.16	0.02	3.12	0.27	2.69

identified in the current study (Table S1) and the interaction of 14-3-3ζ with HSP70 was further confirmed by coimmunoprecipitation and colocalization analysis (Figures 4 and 5). Intriguingly, our confocal immunofluorescence analyses demonstrated that 14-3-3ζ colocalized with BAG3 in U266 cells. These data, along with the results on 14-3-3ζ/BAG3 coimmu-

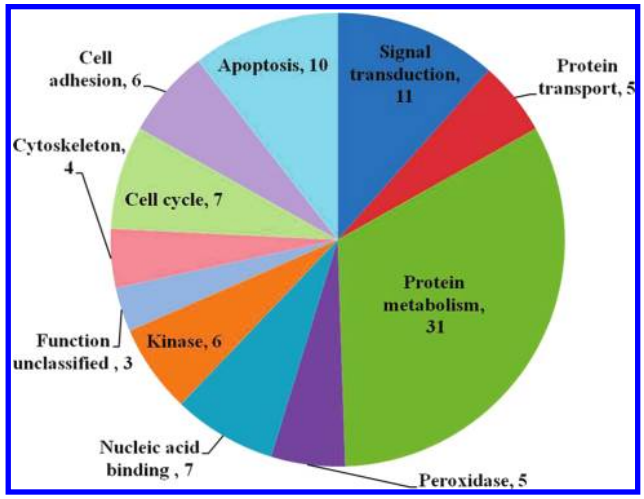

Figure 3. Functional distribution of novel 14-3-3ζ interacting proteins. Categorizations were based on information provided by the online resource PANTHER classification system.

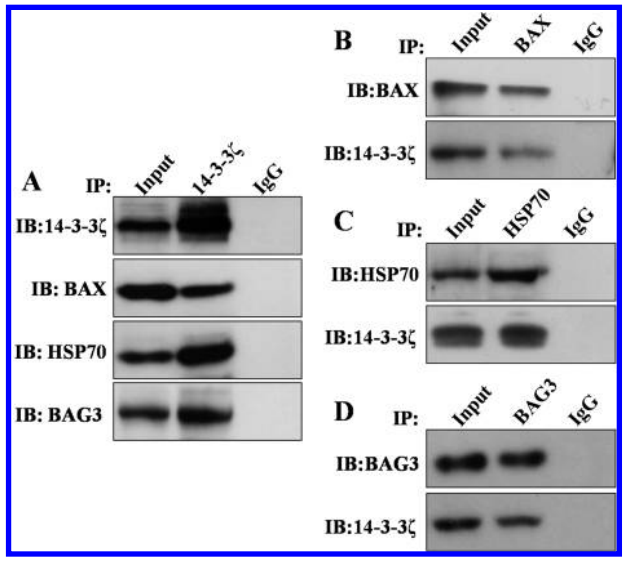

Figure 4. Immunoblot analysis after coimmunoprecipitation assay. Immunoprecipitation assays of 14-3-3ζ, BAX, HSP70, and BAG3 proteins were carried out in U266 cells as described in Experimental Procedures. (A) Immunoblot analysis demonstrated that 14-3-3ζ protein binds with BAX, HSP70, and BAG3 proteins. No band of 14-3-3ζ was observed in the negative control (IgG). Input stands for the total cell lysate extracted from U266 cells. Similarly, reverse immunoprecipitation assays confirmed the binding of (B) BAX, (C) HSP70, and (D) BAG3 protein with 14-3-3ζ.

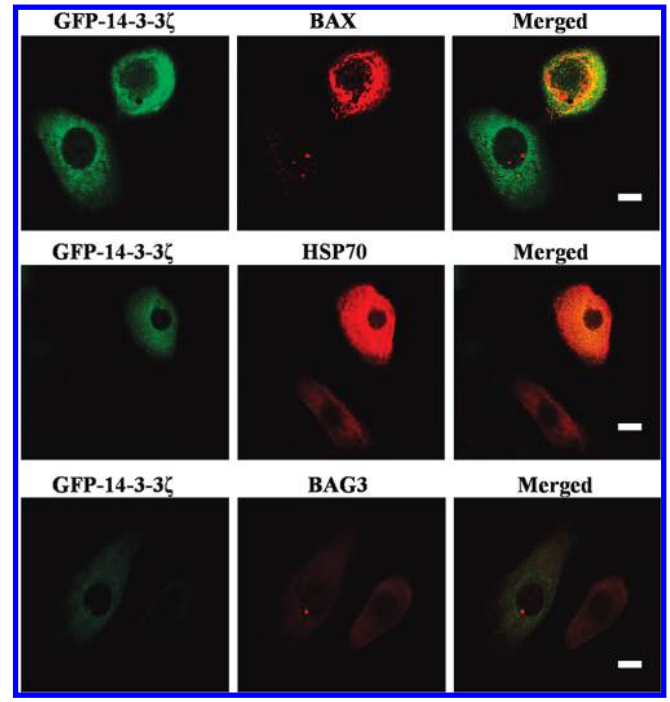

Figure 5. Colocalization of 14-3-3ζ with BAX, HSP70, and BAG3 in U266 cells. U266 cells were transfected with pEGFP-14-3-3ζ expression plasmids and maintained for 24 h, fixed, and stained with anti-BAX, -HSP70, or -BAG3 antibodies that were detected with fluorescent secondary antibody. Images for 14-3-3ζ and BAX, HSP70, BAG3 were collected on a confocal microscope and colocalization analysis was performed using IMAGE J software. Scale bar: 10 μm.

Table 2. Colocalization Analysis of 14-3-3ζ with BAX, HSP70, and BAG3

protein pair	Mander's coefficients[a]	Pearson's *R*		Costes' randomization	
		R^b	*R*(rand)[c]	iterations	*R* > *R*(rand)[d]
14-3-3ζ/BAX	0.86 ± 0.11	0.656	0.004	3000	100%
14-3-3ζ/HSP70	0.67 ± 0.09	0.865	0.005	3000	100%
14-3-3ζ/BAG3	0.71 ± 0.10	0.810	−0.003	3000	100%

[a] Manders coefficient indicates the actual overlap of the signals and values over 0.6 are considered to represent colocalization.[37,75] [b] The Pearson's coefficient describes the correlation of the intensity distribution between channels and varies from −1 to +1. Values over +0.5 are considered as indicative of colocalization.[37,75] [c] *R*(rand): mean of Pearson's correlation coefficients obtained from randomized images by Costes' method. Costes' method for randomization involves generating scrambled images by randomly rearranging blocks in one of the channels (in a Monte Carlo fashion) for specified iterations (3000 in this case). Pearson's *R* is calculated for each and the mean is stated as *R*(rand). [d] *R* > *R*(rand): number of times the actual Pearson's *R* is greater than the random *R*, within the number of iterations performed.

noprecipitation, support the idea that 14-3-3ζ interacts with both types of chaperones and raise the possibility that 14-3-3ζ may form an *in vivo* complex with HSP70 and BAG3.

The association of 14-3-3ζ with HSP70 and BAG3 appears to be a remarkable feature of this protein. It has been demonstrated that 14-3-3ζ proteins are involved in regulating cytoskeletal architecture and controlling cellular morphology.[50] Recent evidence also demonstrated that BAG3 can regulate the actin-cytoskeleton and control cell motility or cell adhesion.[51,52] It has been proposed that BAG3 regulates cell motility by recruiting HSP70 to other BAG3-interacting proteins on the actin cytoskeleton and modulating HSP70 chaperone activity.[52]

Therefore, it is likely that the interaction of 14-3-3ζ with BAG3 and HSP70 may regulate the stability and dynamics of cytoskeleton. It is also possible that such interactions may be dynamically regulated by stimuli in coordination with the diverse functions of these proteins during cellular processes such as cell survival (stress response), proliferation, migration, and apoptosis. Therefore, the interaction of 14-3-3ζ with BAG3 and HSP70 appears to represent a novel mechanism for maintaining the stability and dynamics of cytoskeleton in MM cells.

It is not clear from our results whether 14-3-3ζ is a cofactor partner of BAG3−HSP70 complex. It is, therefore, tempting to speculate that the physiological interaction between these proteins might contribute to the cooperation and/or coordination of their functions in the control of numerous intracellular

signaling and regulatory pathways. Further work is ongoing that combines individual knockouts of BAG3, HSP70, and 14-3-3 proteins with quantitative proteomics to clarify the role of these proteins in myeloma cells.

Ten novel 14-3-3ζ interacting proteins belong to the apoptosis class, including three caspases and BCL2-associated X protein (BAX). BAX, a member of Bcl-2 family, plays an essential role in apoptotic pathways induced by a number of apoptotic stimuli.[53] The Bcl-2 family proteins play a critical role in the apoptotic process. Among the Bcl-2 family proteins, BAX is thought to be the most important pro-apoptotic protein.[54−56] Upon apoptotic stimuli, BAX undergoes a conformational change, translocates to the outer mitochondrial membrane,[57] and permeabilizes the mitochondrial membrane to release apoptotic factors.[58] Currently, there is a great interest in understanding how the BAX activity is regulated during apoptosis. It has been shown that several proteins, including Mcl-1, Ku70, and Humanin, sequester BAX in the cytoplasm.[59−61]

It is noteworthy that the 14-3-3 proteins were found to play a crucial inhibitory role in regulating BAX activity.[60,62] Consistent with these reports, we have shown that the apoptosis induced by the 14-3-3ζ knockdown appeared to be mediated in part by up-regulated Bad and BAX.[63] However, the precise role of 14-3-3ζ in the regulation of BAX responses to apoptotic stimulus in MM cells remains unclear.

In this study, both proteomic and biochemical results clearly showed that BAX is a 14-3-3ζ-associated protein. Most of the proteins that interact with 14-3-3 proteins do so via phosphorylated serine or threonine residues.[64] Therefore, the possibility exists that BAX is bound to 14-3-3ζ in MM cells, and an unidentified phosphoprotein(s) interacts with 14-3-3ζ to release BAX from the complex after delivery of an apoptotic stimulus. Recently, a caspase-activation-independent mechanism for the dissociation of BAX from 14-3-3 was described, whereby c-Jun N-terminal kinase (JNK) promotes BAX translocation to mitochondria by phosphorylating 14-3-3.[65,66] Furthermore, it has been reported that the JNK inhibitor significantly attenuated the cyclin-dependent kinase inhibitor flavopiridol and the small-molecule Bcl-2 antagonist HA14−1-mediated lethality in MM cells indicates that JNK activation plays at least some functional role in apoptosis induction.[67] The mechanism by which JNK activation exerts proapoptotic actions is not known with certainty but may be related to promotion of cytochrome c release[68] as well as phosphorylation and inactivation of antiapoptotic proteins such as Bcl-2[69] and Mcl-1.[70]

On the basis of the important role of 14-3-3ζ and JNK pathway in myeloma growth and survival,[63,71,72] we speculate that JNK mediated phosphorylation of 14-3-3ζ in conjunction with the dissociation of BAX from 14-3-3ζ, at least in part, may contribute to the induced apoptosis in MM cells. This speculative idea, however, is not yet supported by experimental data, and in-depth analysis of these interactions is currently underway to elucidate their functional significance in MM cells.

It is important to note that several 14-3-3 isoforms were copurified with 14-3-3ζ, which is in accordance with previous reports showing heterodimerization between different 14-3-3 isoforms.[73,74] Therefore, it is possible that some of the 14-3-3ζ-associated proteins identified in this study do not directly interact with 14-3-3ζ but with other 14-3-3 isoforms directly binding to 14-3-3ζ. As our affinity purification approach allows the purification of protein complexes, some of the identified 14-3-3ζ-associated proteins may be components of multiprotein complexes and therefore may not directly interact with 14-3-3ζ. Whether each interaction is direct remains to be examined for many of the identified novel interactors. We are currently using parallel proteomic studies comparing the ligands associated with different 14-3-3 isoforms under identical conditions to address this issue.

The identified novel proteins categorized into other functional groups include signal transduction (12%), nucleic acid binding (8%), protein transport (5%), peroxidase (5%), kinase (6%), cytoskeleton (4%), cell adhesion (6%), and cell cycle (7%). Other identified proteins with their subfamilies not being classified were categorized as "function unclassified " (3%).

In summary, we described QUICK as a powerful method for quantitative analysis of protein interactions by mass spectrometry. By using this unambiguous approach, we systematically profiled multiple proteins interacting with 14-3-3ζ in myeloma cells. Many reliable 14-3-3ζ interacting proteins were identified and some interesting clues were given. It is now important to further characterize the interactions between the 14-3-3ζ and individual target proteins and to define the signal transduction pathways that control binding of 14-3-3ζ to their multiple binding partners in response to changing physiological conditions.

Abbreviations: MM, multiple myeloma; QUICK, quantitative immunoprecipitation combined with knockdown; SILAC, stable isotope labeling by amino acids in cell culture; BAX, BCL2-associated X protein; BAG3, BCL2-associated athanogene 3; HSP, heat shock protein; PANTHER, Protein analysis through evolutionary relationships; PPIs, protein−protein interactions.

Acknowledgment. This work was supported by Hundred Talents Program of The Chinese Academy of Sciences, the National Protein Research Fund (Grant No: 2009CB825400 and 2006CB910902), the Infectious Diseases Control Project from Ministry of Health of China (No. 2009ZX10004-107), the Major Special Program on Infectious Diseases from Ministry of Health of China (2008ZX10003-005), the State Key Development Program for Basic Research of China (Grant No. 2010CB529205) and a Grant-in-Aid for Scientific Research from Japan Society for the Promotion of Science.

Supporting Information Available: Tables S1−S5; list of identified 14-3-3ζ interacting proteins (SI ≥ 2); list of proteins which are nonspecific binding to 14-3-3ζ (SI < 2); sequences and normalized abundance ratios of the quantified peptides in siRNA group; sequences and normalized abundance ratios of the quantified peptides in control group; list of known interacting proteins for 14-3-3ζ. This material is available free of charge via the Internet at http://pubs.acs.org.

References

(1) Fu, H.; Subramanian, R. R.; Masters, S. C. 14-3-3 proteins: structure, function, and regulation. *Annu. Rev. Pharmacol. Toxicol.* **2000**, *40*, 617–47.
(2) Aitken, A. 14-3-3 proteins: a historic overview. *Semin. Cancer Biol.* **2006**, *16* (3), 162–72.
(3) Muslin, A. J.; Lau, J. M. Differential functions of 14-3-3 isoforms in vertebrate development. *Curr. Top. Dev. Biol.* **2005**, *65*, 211–28.
(4) Morrison, D. K. The 14-3-3 proteins: integrators of diverse signaling cues that impact cell fate and cancer development. *Trends Cell Biol.* **2009**, *19* (1), 16–23.
(5) Wilker, E.; Yaffe, M. B. 14-3-3 proteins—a focus on cancer and human disease. *J. Mol. Cell. Cardiol.* **2004**, *37* (3), 633–42.
(6) Tzivion, G.; Shen, Y. H.; Zhu, J. 14-3-3 proteins; bringing new definitions to scaffolding. *Oncogene* **2001**, *20* (44), 6331–8.

(7) Shen, Y. H.; Godlewski, J.; Bronisz, A.; Zhu, J.; Comb, M. J.; Avruch, J.; Tzivion, G. Significance of 14-3-3 self-dimerization for phosphorylation-dependent target binding. *Mol. Biol. Cell* **2003**, *14* (11), 4721–33.

(8) Coblitz, B.; Wu, M.; Shikano, S.; Li, M. C-terminal binding: an expanded repertoire and function of 14-3-3 proteins. *FEBS Lett.* **2006**, *580* (6), 1531–5.

(9) Thomas, D.; Guthridge, M.; Woodcock, J.; Lopez, A. 14-3-3 protein signaling in development and growth factor responses. *Curr. Top. Dev. Biol.* **2005**, *67*, 285–303.

(10) Powell, D. W.; Rane, M. J.; Joughin, B. A.; Kalmukova, R.; Hong, J. H.; Tidor, B.; Dean, W. L.; Pierce, W. M.; Klein, J. B.; Yaffe, M. B.; McLeish, K. R. Proteomic identification of 14-3-3zeta as a mitogen-activated protein kinase-activated protein kinase 2 substrate: role in dimer formation and ligand binding. *Mol. Cell. Biol.* **2003**, *23* (15), 5376–87.

(11) Jin, Z.; Gao, F.; Flagg, T.; Deng, X. Nicotine induces multi-site phosphorylation of Bad in association with suppression of apoptosis. *J. Biol. Chem.* **2004**, *279* (22), 23837–44.

(12) Porter, G. W.; Khuri, F. R.; Fu, H. Dynamic 14-3-3/client protein interactions integrate survival and apoptotic pathways. *Semin. Cancer Biol.* **2006**, *16* (3), 193–202.

(13) Chiang, C. W.; Kanies, C.; Kim, K. W.; Fang, W. B.; Parkhurst, C.; Xie, M.; Henry, T.; Yang, E. Protein phosphatase 2A dephosphorylation of phosphoserine 112 plays the gatekeeper role for BAD-mediated apoptosis. *Mol. Cell. Biol.* **2003**, *23* (18), 6350–62.

(14) Tzivion, G.; Avruch, J. 14-3-3 proteins: active cofactors in cellular regulation by serine/threonine phosphorylation. *J. Biol. Chem.* **2002**, *277* (5), 3061–4.

(15) Rena, G.; Prescott, A. R.; Guo, S.; Cohen, P.; Unterman, T. G. Roles of the forkhead in rhabdomyosarcoma (FKHR) phosphorylation sites in regulating 14-3-3 binding, transactivation and nuclear targetting. *Biochem. J.* **2001**, *354*, 605–12.

(16) Cahill, C. M.; Tzivion, G.; Nasrin, N.; Ogg, S.; Dore, J.; Ruvkun, G.; Alexander-Bridges, M. Phosphatidylinositol 3-kinase signaling inhibits DAF-16 DNA binding and function via 14-3-3-dependent and 14-3-3-independent pathways. *J. Biol. Chem.* **2001**, *276* (16), 13402–10.

(17) Li, X.; Song, S.; Liu, Y.; Ko, S. H.; Kao, H. Y. Phosphorylation of the histone deacetylase 7 modulates its stability and association with 14-3-3 proteins. *J. Biol. Chem.* **2004**, *279* (33), 34201–8.

(18) Hermeking, H.; Benzinger, A. 14-3-3 proteins in cell cycle regulation. *Semin. Cancer Biol.* **2006**, *16* (3), 183–92.

(19) van Hemert, M. J.; Steensma, H. Y.; van Heusden, G. P. 14-3-3 proteins: key regulators of cell division, signalling and apoptosis. *BioEssays* **2001**, *23* (10), 936–46.

(20) Rodriguez, L. G.; Guan, J. L. 14-3-3 regulation of cell spreading and migration requires a functional amphipathic groove. *J. Cell Physiol.* **2005**, *202* (1), 285–94.

(21) Muslin, A. J.; Tanner, J. W.; Allen, P. M.; Shaw, A. S. Interaction of 14-3-3 with signaling proteins is mediated by the recognition of phosphoserine. *Cell* **1996**, *84* (6), 889–97.

(22) Rittinger, K.; Budman, J.; Xu, J.; Volinia, S.; Cantley, L. C.; Smerdon, S. J.; Gamblin, S. J.; Yaffe, M. B. Structural analysis of 14-3-3 phosphopeptide complexes identifies a dual role for the nuclear export signal of 14-3-3 in ligand binding. *Mol. Cell* **1999**, *4* (2), 153–66.

(23) Ganguly, S.; Weller, J. L.; Ho, A.; Chemineau, P.; Malpaux, B.; Klein, D. C. Melatonin synthesis: 14-3-3-dependent activation and inhibition of arylalkylamine N-acetyltransferase mediated by phosphoserine-205. *Proc. Natl. Acad. Sci. U.S.A.* **2005**, *102* (4), 1222–7.

(24) Aitken, A. Functional specificity in 14-3-3 isoform interactions through dimer formation and phosphorylation. Chromosome location of mammalian isoforms and variants. *Plant Mol. Biol.* **2002**, *50* (6), 993–1010.

(25) Henriksson, M. L.; Francis, M. S.; Peden, A.; Aili, M.; Stefansson, K.; Palmer, R.; Aitken, A.; Hallberg, B. A nonphosphorylated 14-3-3 binding motif on exoenzyme S that is functional in vivo. *Eur. J. Biochem.* **2002**, *269* (20), 4921–9.

(26) Zhai, J.; Lin, H.; Shamim, M.; Schlaepfer, W. W.; Canete-Soler, R. Identification of a novel interaction of 14-3-3 with p190RhoGEF. *J. Biol. Chem.* **2001**, *276* (44), 41318–24.

(27) Tian, Q.; Feetham, M. C.; Tao, W. A.; He, X. C.; Li, L.; Aebersold, R.; Hood, L. Proteomic analysis identifies that 14-3-3zeta interacts with beta-catenin and facilitates its activation by Akt. *Proc. Natl. Acad. Sci. U.S.A.* **2004**, *101* (43), 15370–5.

(28) Li, Z.; Zhao, J.; Du, Y.; Park, H. R.; Sun, S. Y.; Bernal-Mizrachi, L.; Aitken, A.; Khuri, F. R.; Fu, H. Down-regulation of 14-3-3zeta suppresses anchorage-independent growth of lung cancer cells through anoikis activation. *Proc. Natl. Acad. Sci. U.S.A.* **2008**, *105* (1), 162–7.

(29) Lu, J.; Guo, H.; Treekitkarnmongkol, W.; Li, P.; Zhang, J.; Shi, B.; Ling, C.; Zhou, X.; Chen, T.; Chiao, P. J.; Feng, X.; Seewaldt, V. L.; Muller, W. J.; Sahin, A.; Hung, M. C.; Yu, D. 14-3-3zeta Cooperates with ErbB2 to promote ductal carcinoma in situ progression to invasive breast cancer by inducing epithelial-mesenchymal transition. *Cancer Cell* **2009**, *16* (3), 195–207.

(30) Ge, F.; Lu, X. P.; Zeng, H. L.; He, Q. Y.; Xiong, S.; Jin, L.; He, Q. Y. Proteomic and functional analyses reveal a dual molecular mechanism underlying arsenic-induced apoptosis in human multiple myeloma cells. *J. Proteome Res.* **2009**, *8* (6), 3006–19.

(31) Selbach, M.; Mann, M. Protein interaction screening by quantitative immunoprecipitation combined with knockdown (QUICK). *Nat. Methods* **2006**, *3* (12), 981–3.

(32) Mann, M. Functional and quantitative proteomics using SILAC. *Nat. Rev. Mol. Cell Biol.* **2006**, *7* (12), 952–8.

(33) Ong, S. E.; Mann, M. A practical recipe for stable isotope labeling by amino acids in cell culture (SILAC). *Nat. Protoc.* **2006**, *1* (6), 2650–60.

(34) Heide, H.; Nordhues, A.; Drepper, F.; Nick, S.; Schulz-Raffelt, M.; Haehnel, W.; Schroda, M. Application of quantitative immunoprecipitation combined with knockdown and cross-linking to Chlamydomonas reveals the presence of vesicle-inducing protein in plastids 1 in a common complex with chloroplast HSP90C. *Proteomics* **2009**, *9* (11), 3079–89.

(35) Saito, A.; Nagasaki, M.; Oyama, M.; Kozuka-Hata, H.; Semba, K.; Sugano, S.; Yamamoto, T.; Miyano, S. AYUMS: an algorithm for completely automatic quantitation based on LC-MS/MS proteome data and its application to the analysis of signal transduction. *BMC Bioinf.* **2007**, *8*, 15.

(36) Mi, H.; Guo, N.; Kejariwal, A.; Thomas, P. D. PANTHER version 6: protein sequence and function evolution data with expanded representation of biological pathways. *Nucleic Acids Res.* **2007**, *35* (Database issue), D247–52.

(37) Bolte, S.; Cordelieres, F. P. A guided tour into subcellular colocalization analysis in light microscopy. *J. Microsc.* **2006**, *224* (Pt. 3), 213–32.

(38) Costes, S. V.; Daelemans, D.; Cho, E. H.; Dobbin, Z.; Pavlakis, G.; Lockett, S. Automatic and quantitative measurement of protein-protein colocalization in live cells. *Biophys. J.* **2004**, *86* (6), 3993–4003.

(39) Sutherland, B. W.; Toews, J.; Kast, J. Utility of formaldehyde cross-linking and mass spectrometry in the study of protein-protein interactions. *J. Mass Spectrom.* **2008**, *43* (6), 699–715.

(40) Toews, J.; Rogalski, J. C.; Clark, T. J.; Kast, J. Mass spectrometric identification of formaldehyde-induced peptide modifications under in vivo protein cross-linking conditions. *Anal. Chim. Acta* **2008**, *618* (2), 168–83.

(41) Doong, H.; Vrailas, A.; Kohn, E. C. What's in the 'BAG'?—A functional domain analysis of the BAG-family proteins. *Cancer Lett.* **2002**, *188* (1−2), 25–32.

(42) Doong, H.; Price, J.; Kim, Y. S.; Gasbarre, C.; Probst, J.; Liotta, L. A.; Blanchette, J.; Rizzo, K.; Kohn, E. CAIR-1/BAG-3 forms an EGF-regulated ternary complex with phospholipase C-gamma and Hsp70/Hsc70. *Oncogene* **2000**, *19* (38), 4385–95.

(43) Rosati, A.; Ammirante, M.; Gentilella, A.; Basile, A.; Festa, M.; Pascale, M.; Marzullo, L.; Belisario, M. A.; Tosco, A.; Franceschelli, S.; Moltedo, O.; Pagliuca, G.; Lerose, R.; Turco, M. C. Apoptosis inhibition in cancer cells: a novel molecular pathway that involves BAG3 protein. *Int. J. Biochem. Cell Biol.* **2007**, *39* (7−8), 1337–42.

(44) Doong, H.; Rizzo, K.; Fang, S.; Kulpa, V.; Weissman, A. M.; Kohn, E. C. CAIR-1/BAG-3 abrogates heat shock protein-70 chaperone complex-mediated protein degradation: accumulation of poly-ubiquitinated Hsp90 client proteins. *J. Biol. Chem.* **2003**, *278* (31), 28490–500.

(45) Gamerdinger, M.; Hajieva, P.; Kaya, A. M.; Wolfrum, U.; Hartl, F. U.; Behl, C. Protein quality control during aging involves recruitment of the macroautophagy pathway by BAG3. *EMBO J.* **2009**, *28* (7), 889–901.

(46) Zhang, L.; Zhang, Z. P.; Zhang, X. E.; Lin, F. S.; Ge, F. Quantitative proteomics analysis reveals BAG3 as a potential target to suppress severe acute respiratory syndrome coronavirus replication. *J. Virol.* **2010**, *84* (12), 6050–9.

(47) Pagliuca, M. G.; Lerose, R.; Cigliano, S.; Leone, A. Regulation by heavy metals and temperature of the human BAG-3 gene, a modulator of Hsp70 activity. *FEBS Lett.* **2003**, *541* (1−3), 11–5.

(48) Nollen, E. A.; Morimoto, R. I. Chaperoning signaling pathways: molecular chaperones as stress-sensing 'heat shock' proteins. *J. Cell Sci.* **2002**, *115* (Pt. 14), 2809–16.

(49) Jolly, C.; Morimoto, R. I. Role of the heat shock response and molecular chaperones in oncogenesis and cell death. *J. Natl. Cancer Inst.* **2000**, *92* (19), 1564–72.
(50) Jin, J.; Smith, F. D.; Stark, C.; Wells, C. D.; Fawcett, J. P.; Kulkarni, S.; Metalnikov, P.; O'Donnell, P.; Taylor, P.; Taylor, L.; Zougman, A.; Woodgett, J. R.; Langeberg, L. K.; Scott, J. D.; Pawson, T. Proteomic, functional, and domain-based analysis of in vivo 14-3-3 binding proteins involved in cytoskeletal regulation and cellular organization. *Curr. Biol.* **2004**, *14* (16), 1436–50.
(51) Kassis, J. N.; Guancial, E. A.; Doong, H.; Virador, V.; Kohn, E. C. CAIR-1/BAG-3 modulates cell adhesion and migration by down-regulating activity of focal adhesion proteins. *Exp. Cell Res.* **2006**, *312* (15), 2962–71.
(52) Iwasaki, M.; Homma, S.; Hishiya, A.; Dolezal, S. J.; Reed, J. C.; Takayama, S. BAG3 regulates motility and adhesion of epithelial cancer cells. *Cancer Res.* **2007**, *67* (21), 10252–9.
(53) Wei, M. C.; Zong, W. X.; Cheng, E. H.; Lindsten, T.; Panoutsakopoulou, V.; Ross, A. J.; Roth, K. A.; MacGregor, G. R.; Thompson, C. B.; Korsmeyer, S. J. Proapoptotic BAX and BAK: a requisite gateway to mitochondrial dysfunction and death. *Science* **2001**, *292* (5517), 727–30.
(54) Lindsten, T.; Zong, W. X.; Thompson, C. B. Defining the role of the Bcl-2 family of proteins in the nervous system. *Neuroscientist* **2005**, *11* (1), 10–5.
(55) Zong, W. X.; Li, C.; Hatzivassiliou, G.; Lindsten, T.; Yu, Q. C.; Yuan, J.; Thompson, C. B. Bax and Bak can localize to the endoplasmic reticulum to initiate apoptosis. *J. Cell Biol.* **2003**, *162* (1), 59–69.
(56) Zong, W. X.; Lindsten, T.; Ross, A. J.; MacGregor, G. R.; Thompson, C. B. BH3-only proteins that bind pro-survival Bcl-2 family members fail to induce apoptosis in the absence of Bax and Bak. *Genes Dev.* **2001**, *15* (12), 1481–6.
(57) Hsu, Y. T.; Wolter, K. G.; Youle, R. J. Cytosol-to-membrane redistribution of Bax and Bcl-X(L) during apoptosis. *Proc. Natl. Acad. Sci. U.S.A.* **1997**, *94* (8), 3668–72.
(58) Nechushtan, A.; Smith, C. L.; Lamensdorf, I.; Yoon, S. H.; Youle, R. J. Bax and Bak coalesce into novel mitochondria-associated clusters during apoptosis. *J. Cell Biol.* **2001**, *153* (6), 1265–76.
(59) Nijhawan, D.; Fang, M.; Traer, E.; Zhong, Q.; Gao, W.; Du, F.; Wang, X. Elimination of Mcl-1 is required for the initiation of apoptosis following ultraviolet irradiation. *Genes Dev.* **2003**, *17* (12), 1475–86.
(60) Sawada, M.; Sun, W.; Hayes, P.; Leskov, K.; Boothman, D. A.; Matsuyama, S. Ku70 suppresses the apoptotic translocation of Bax to mitochondria. *Nat. Cell Biol.* **2003**, *5* (4), 320–9.
(61) Guo, B.; Zhai, D.; Cabezas, E.; Welsh, K.; Nouraini, S.; Satterthwait, A. C.; Reed, J. C. Humanin peptide suppresses apoptosis by interfering with Bax activation. *Nature* **2003**, *423* (6938), 456–61.
(62) Nomura, M.; Shimizu, S.; Sugiyama, T.; Narita, M.; Ito, T.; Matsuda, H.; Tsujimoto, Y. 14-3-3 Interacts directly with and negatively regulates pro-apoptotic Bax. *J. Biol. Chem.* **2003**, *278* (3), 2058–65.
(63) Ge, F.; Lu, X. P.; Zeng, H. L.; He, Q. Y.; Xiong, S.; Jin, L. Proteomic and functional analyses reveal a dual molecular mechanism underlying arsenic-induced apoptosis in human multiple myeloma cells. *J. Proteome Res.* **2009**, *8* (6), 3006–19.
(64) Aitken, A. 14-3-3 and its possible role in co-ordinating multiple signalling pathways. *Trends Cell Biol.* **1996**, *6* (9), 341–7.
(65) Tsuruta, F.; Sunayama, J.; Mori, Y.; Hattori, S.; Shimizu, S.; Tsujimoto, Y.; Yoshioka, K.; Masuyama, N.; Gotoh, Y. JNK promotes Bax translocation to mitochondria through phosphorylation of 14-3-3 proteins. *EMBO J.* **2004**, *23* (8), 1889–99.
(66) Sunayama, J.; Tsuruta, F.; Masuyama, N.; Gotoh, Y. JNK antagonizes Akt-mediated survival signals by phosphorylating 14-3-3. *J. Cell Biol.* **2005**, *170* (2), 295–304.
(67) Pei, X. Y.; Dai, Y.; Grant, S. The small-molecule Bcl-2 inhibitor HA14−1 interacts synergistically with flavopiridol to induce mitochondrial injury and apoptosis in human myeloma cells through a free radical-dependent and Jun NH2-terminal kinase-dependent mechanism. *Mol. Cancer Ther.* **2004**, *3* (12), 1513–24.
(68) Tournier, C.; Hess, P.; Yang, D. D.; Xu, J.; Turner, T. K.; Nimnual, A.; Bar-Sagi, D.; Jones, S. N.; Flavell, R. A.; Davis, R. J. Requirement of JNK for stress-induced activation of the cytochrome c-mediated death pathway. *Science* **2000**, *288* (5467), 870–4.
(69) Yamamoto, K.; Ichijo, H.; Korsmeyer, S. J. BCL-2 is phosphorylated and inactivated by an ASK1/Jun N-terminal protein kinase pathway normally activated at G(2)/M. *Mol. Cell. Biol.* **1999**, *19* (12), 8469–78.
(70) Inoshita, S.; Takeda, K.; Hatai, T.; Terada, Y.; Sano, M.; Hata, J.; Umezawa, A.; Ichijo, H. Phosphorylation and inactivation of myeloid cell leukemia 1 by JNK in response to oxidative stress. *J. Biol. Chem.* **2002**, *277* (46), 43730–4.
(71) Colla, S.; Zhan, F.; Xiong, W.; Wu, X.; Xu, H.; Stephens, O.; Yaccoby, S.; Epstein, J.; Barlogie, B.; Shaughnessy, J. D., Jr. The oxidative stress response regulates DKK1 expression through the JNK signaling cascade in multiple myeloma plasma cells. *Blood* **2007**, *109* (10), 4470–7.
(72) Wen, J.; Feng, Y.; Huang, W.; Chen, H.; Liao, B.; Rice, L.; Preti, H. A.; Kamble, R. T.; Zu, Y.; Ballon, D. J.; Chang, C. C. Enhanced antimyeloma cytotoxicity by the combination of arsenic trioxide and bortezomib is further potentiated by p38 MAPK inhibition. *Leuk. Res.* **2010**, *34* (1), 85–92.
(73) Chaudhri, M.; Scarabel, M.; Aitken, A. Mammalian and yeast 14-3-3 isoforms form distinct patterns of dimers in vivo. *Biochem. Biophys. Res. Commun.* **2003**, *300* (3), 679–85.
(74) Benzinger, A.; Muster, N.; Koch, H. B.; Yates, J. R., 3rd; Hermeking, H. Targeted proteomic analysis of 14-3-3 sigma, a p53 effector commonly silenced in cancer. *Mol. Cell. Proteomics* **2005**, *4* (6), 785–95.
(75) Zinchuk, V.; Zinchuk, O. Quantitative colocalization analysis of confocal fluorescence microscopy images. *Curr. Protoc. Cell Biol.* **2008**, *39*, 4.19.1−4.19.16.

PR100616G